

Understanding process-structure-property relation for elastoplastic behavior of polymer nanocomposites with agglomeration anomalies and gradient interphase percolation

Prajakta Prabhune^a, Anlan Chen^a, Yigitcan Comlek^b, Wei Chen^b, L. Catherine Brinson^{a,*}

^a*Thomas Lord Department of Mechanical Engineering and Materials Science, Duke University, Durham, USA*

^b*Department of Mechanical Engineering, Northwestern University, Evanston, USA*

Abstract

Polymer nanocomposites are inherently tailorable materials and capable of providing higher strength to weight ratio than traditional hard metals. However, their disordered microstructural nature makes processing control and hence tailoring properties to desired values a challenge. Additionally, interfacial region, also called interphase, is a key material phase in these heterogeneous materials and its extent depends on variety of microstructural features like dispersion. Understanding process-structure-property (PSP) relation can provide guidelines for process and constituents' design. Our work explores nuances of PSP relation for polymer nanocomposites with attractive pairing between particles and polymer bulk. Past works have shown that particle functionalization can help tweak these interactions in attractive or repulsive directions and can produce slow or fast decay of stiffness properties in polymer nanocomposites. In absence of any nano or micro-scale local property measurement, we develop a material model that can represent decay for small strain elastoplastic (Young's modulus and yield strength) properties in interfacial regions and simulate representative or statistical volume element behavior. The interfacial elastoplastic material model is devised by combining local stiffness and glass transition measurements that were obtained by previous researchers by atomic force microscopy and fluorescence microscopy. This is further combined with a microstructural design of experiments for agglomerated nanocomposite systems. Agglomerations are particle aggregations that are processing artefacts that result from lack of processing control. Twin screw extrusion process can reduce extent of aggregation in hot pressed samples via erosion or rupture depending on screw rpms and torque. We connect this process-structure relation to structure-property relation that emerges from our study. We discover that balancing between local stress concentration zones (SCZ) and interfacial property decay governs how fast yield stress can improve if we break down agglomeration via erosion. Rupture is relatively less effective in helping improve nanocomposite yield strength. We also observe an inflexion point where incremental increase brought on by rupture is slowed down due to increasing SCZ and saturation in interphase percolation.

Keywords:

1. Introduction

1.1. Motivation and background

Understanding process-structure-property relation for polymer nanocomposites is fundamental to design and manufacture of these advanced heterogeneous and disordered materials in variety of technology domains. For the ease of their handling and high strength to weight ratio, 3D printing processes are increasingly using polymer nanocomposites for fabricating precision components used in mechanical, electrical, electronics, electrochemical and nanomedicine systems. Characterising elastoplastic material properties of nanocomposites is critical from the perspective of design of components for structural integrity and load bearing purposes.

However, it has been a challenge to characterise elastoplastic behaviour of nanocomposites at bulk and nanoscale due to lack of process control, difficulties characterising 3D microstructure of the materials systems, and time and effort involved in systematic experimentation to characterize properties of an extensive number of samples. Combining computational mechanics and statistically equivalent artificial microstructure reconstructions can be used to overcome these challenges and develop insight into behavior and tools for design.

Nanocomposites are multiphase materials with individual phases at nano or microscale and their distribution throughout the medium determine the final properties in a complex manner. Nanoscale particles with higher modulus can themselves provide stiffening effects to the medium. If particle-particle interaction is relatively attractive compared to polymer-particle interaction, they tend to form larger, up to micro-sized particle aggregates called agglomerations during nanoparticle synthesis as well as nanocomposite manufacturing process [1, 2, 3, 4]. Agglomerations are considered particle dispersion anomalies that results due to lack of processing control. Past research has witnessed a transition from brittle to ductile behaviour in nanocomposite mechanical properties that accompanies transition in particle aggregate size from a fraction of micrometer to a few nanometers [5, 6, 7].

Multiple approaches have been attempted to explain these observed property trends. Two broad categories these approaches occupy are top-down and bottom-up approach. In top-down approaches, micromechanics theories are modified to account for the presence of microstructural anomalies such as aggregates and agglomerations; interracial effects such as interfacial adhesion/debonding and interphase properties. These modifications are in the form of model or material parameters which are deduced by fitting the model against available test data. Often, such approaches are limited by their inability to capture local effects like local property decay in interphase region, local variation in particle dispersion and volume fraction and their effect on interphase percolation. For this very reason, these studies have been able to predict linear properties very well but not nonlinear ones. They show a significant gap between predictions and experiments for nonlinear properties such as yield and tensile since local effects are more prominent in determining effective yielding and failure. Additionally, most of the parameters in such models are empirical and no physical

*Corresponding author

Email address: `cate.brinson@duke.edu` (L. Catherine Brinson)

meaning can be easily attached to these. Thus such parameters are not useful for developing any mechanistic insight into material behavior.

On the contrary, bottom-up approaches try to combine phenomenological micro-mechanical knowledge with nanoscale measurements or numerical simulations to inform modelling through scales.

At the same time, presence of particles and particle aggregates can also give rise to local stress concentrations. Additionally, particle dispersion through the matrix governs how the local field concentrations interact and affect the overall stress distribution. Stress concentrations at macroscale are widely known to have detrimental effects on properties like fatigue and fracture limits. Overall, these behaviours underline the importance of understanding effects from the presence of agglomeration on material system properties.

An especially important and poorly understood phenomenon is the impact of particle dispersion and aggregation on the percolation of interfacial interactions and their effect on both local and global properties. Local changes in polymer properties near particles are usually represented by an intrinsic material phase called the interphase with modified material properties derived from base polymer properties. Experimental characterization efforts at nano and microscale have established that interfacial interactions and geometric confinement cause altered polymer chain mobility in this region resulting in altered physical material properties, including glass transition temperature, elastic modulus, and dielectric constant. Several attempts have been made to experimentally characterize local property variations at both nano and microscale [8, 9, 10, 11, 12, 13, 14]. Atomic Force Microscopy (AFM) characterization of the local modulus on sandwich model composites has established a gradual property decay away, up to a few hundred nanometers, from the interface between matrix and particle, and non-trivial compounding in the interphase region [13, 15]. Li et al. incorporated this understanding in a 2D interphase model for dispersed nanocomposite systems [10]. This model assumes gradient interphase for each particle with multibody compounding effect to simulate elastic and frequency-based viscoelastic properties of nanocomposite samples. modelled by equations below [10]

$$\overline{E}_{d_n} = \alpha' e^{-\beta' d_n} + 1 \quad (1)$$

$$\overline{E}_{compound} = \eta' \left[\sum_{n=1}^N (\overline{E}_{d_n} - 1) \right] + \zeta' + 1 \quad (2)$$

Here, equation 1 computes gradient decay of properties with respect to interface of a single isolated particle or a single agglomeration. Equation 2 compounds effect of two or more isolated particles and/or agglomerations. \overline{E}_{d_n} and $\overline{E}_{compound}$ are normalized moduli as a function of distance d_n from the interface of aggregate number n . Parameters α' and β' define the exponential decay characteristic of single body interphase, such as the extent of interphase and maximum value. Parameters η' and ζ' are scaling and offset values for compound effect. Figure 1 shows interphase images of single body effect and multi-body

compound effect reconstructed by above computations for normalized property profile for one, two and three particles. The parameter set $\alpha', \beta', \eta', \zeta'$ was inferred from the AFM modulus profile from a typical experiment for a thermoplastic. This material model was further used to simulate elastic, and frequency based viscoelastic properties of nanocomposite samples [10, 16]. Effective properties of the material system depend on a complex interplay between these mechanisms. Hence it is vital to capture these details in a computational modelling approach to be able to compute and predict properties accurately. On top of that, capturing how these microscale effects amount through different scales adds an extra layer of complexity to the problem.

To simulate inelastic material behavior, we need stress-strain data beyond the linear regime like yield point data, tangent modulus, and ultimate point values for defining fracture. Local measurements of such data at nanoscale are challenging for a model or real nanocomposites as a controlled sample needs to be prepared with a dispersion characterization. Previous studies on characterizing the local material behaviors are limited to polymer itself [17, 18]. To the best of the authors' knowledge, there is no such data available yet that can be used to infer local non-linear mechanical property variations in nanocomposite material system. Hence, in this work, we combine our understanding of local elastic modulus data, the effect of interfacial interactions on molecular mobility, and the glass transition temperature on the macroscopic non-linear mechanical behavior of amorphous polymers to model the inelastic behavior of the interphase.

In this work, we form an understanding of how microstructure parameters such as particle volume fraction, volume fraction forming agglomerations and number of agglomerations is related to effective nanocomposite properties. We then attempt to connect this structure-property relation to process-structure relation. This helped us gain insights on what is favourable, in terms of structural and processing parameters and make recommendations about what to avoid and what to pursue.

2. Methods

In this section we first describe our elastoplastic interphase model based on local stiffness and Tg gradient measurements from sandwich model nanocomposite (section 2.1). Then we explain the method we use to generate artificial microstructure that are statistically equivalent and can serve a purpose of being a statistical volume element (SVE) for the material system in consideration (section 2.2). Further in section 2.3, we describe interphase percolation schemes of coupled and decoupled gradient interphase and equivalent uniform interphase. We have incorporated multiple schemes in our study for the purpose of comparison and making recommendation for the interphase representations in computer models. In this section, we also interpret the SVE matrix we simulate and analyse to understand trends in property data with respect to microstructural parameters.

2.1. Inelastic Interphase material Model

In the absence of local property data beyond the linear material regime for polymer nanocomposites, we utilize data from local elastic modulus measurement to infer the effect

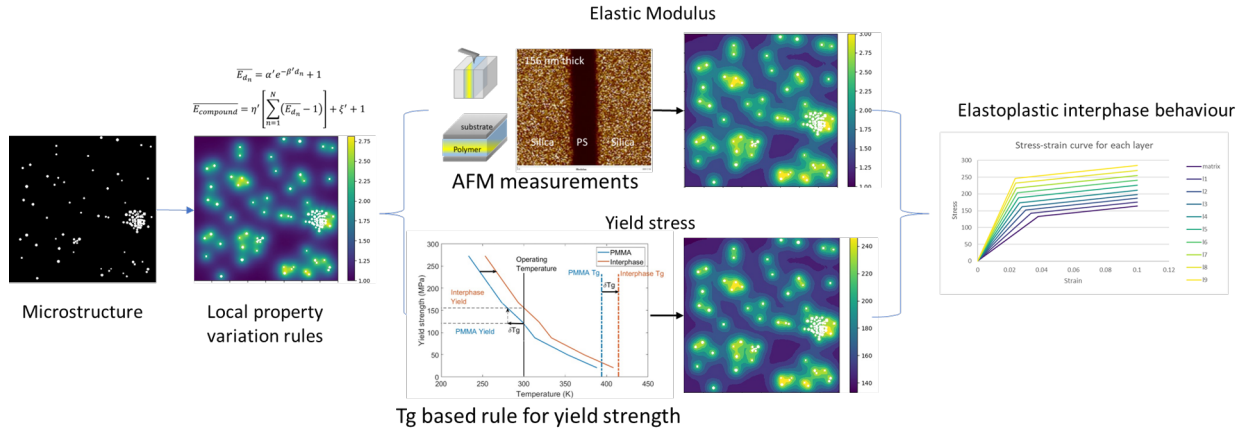


Figure 1: Elasto-plastic interphase model

of interfacial interactions on molecular mobility and glass transition temperature and ultimately to propose a material model for inelastic (yield) properties of the interphase. There have been multiple experimental studies that have tried to quantify the effect of operating temperatures on the macroscopic mechanical behavior of neat polymers. They all point to the fact that the stress-strain behavior of macroscopic polymers under mechanical loading greatly depends on operating temperatures relative to their glass transition temperatures. It has been specifically observed for amorphous polymers that modulus in the linear regime, yield stress decreases, and initial hardening in the nonlinear regime begins to diminish as operating temperatures approach glass transition temperature. A cooperative model of yield process rooted in molecular theories has been proposed and refined through the cumulative work of multiple researchers over the years. This model states that the yield process involves the cooperative motion of chain segments governed by glass transition temperatures, T_g , and molecular mobility. At temperatures below T_g , the polymer chains do not have enough thermal energy and mobility to undergo cooperative movements and act stiffer, recording higher yield stress values but exhibiting brittle failure. On the other hand, at temperatures approaching or above T_g , thermal energy, and mobility can afford cooperative chain movements and record lower yield values along with more ductile failure and high toughness.

We use this understanding to propose a temperature shift model that can be used to derive interphase material properties based on polymer bulk property data. Here we use yield stress as a sample property to explain the model. As explained by the cooperative model, the yield strength drops as the use temperature approaches the polymer glass transition temperature. If we assume attractive interfacial interactions, the polymer in the interphase region exhibits reduced chain mobility and overall reduction and delay in cooperative chain movements. This change would correspond to an increase in the extent of the linear regime and push the yield stress value upwards. We assume that the amount by which polymer yield stress can increase in the interphase region is related to the local change in T_g of the interfacial region polymer. Thus, the yield-temperature curve of interphase can be obtained by shifting the same for neat polymer by amount and direction of change in T_g (see Figure

1(a)). Delta Tg and Young’s modulus are calculated directly by gradient interphase equation, then yield stress can be determined by Substituting into the yield-yemperature curve. A bi-linear model is utilized to define elastoplastic property in Interphase area. Continuous property values are digitized into bins and for each bin, Young’s modulus and yield stress form a bi-linear curve, as depicted in Fig.1(b)

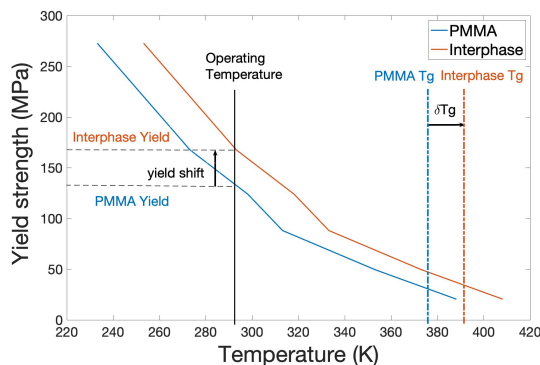


Figure 2: (a)Yield strength-temperature relationship of matrix (measured, CITATION HERE) and our model for the interphase. Our assumption is that the effective glass transition temperature for the interphase is shifted from the matrix by δT_g , shown in the red curve. Thus, for the same operating temperature, the interphase will have a higher yield strength (indicated by arrows) (b) Bi-linear model used to describe the elastoplastic property for the matrix and interphase. The continuous gradient of the interphase is digitized into 9 bins in our example, with bin1 representing material far from the nanofillers and with properties closest to that of the matrix and bin9 is the portion of interphase closest to nanofillers and displaying the largest change in its local mobility and Tg including the compound effect

Conceptually, a similar approach can be adopted to derive other key properties in inelastic or non-linear deformation regimes. For example, strain hardening or softening beyond yield measured tangent modulus. Such extrapolations will require a detailed understanding of underlying molecular processes and how they are being altered within the interphase region by interfacial interactions. This is a topic of extensive and independent research that can combine molecular mobility theories and constitutive modeling at the macroscopic level. For the current purpose of broader and across-the-scale method development, we simplify our approach to selecting from available macroscopic property data that comes from extensive experimental research work about the effect of temperature on the stress-strain relation of polymer materials.

2.2. Characterization and reconstruction of the microstructure with agglomerated particles

Microstructure characterization and reconstruction plays a crucial role in understanding the system [19]. For the system of interest, the key microstructure feature is the presence of nanoparticle agglomerations. Therefore, the characterization and reconstruction revolve around describing the agglomeration features. The system can be characterized by the physical descriptors of total volume fraction (VF), number of agglomerations, and volume fraction of agglomerations present in the system. The difference in the total and agglomeration volume fraction describes the amount of isolated particles present in the system. Considering

the characterization requirements, we implemented a sequential random adsorption inspired approach that involves adding particles to a new microstructure incrementally to reconstruct the material system. We considered a system size of $1 \mu\text{m} \times 1 \mu\text{m}$ and reconstructed it on a 400×400 pixel image. Given total VF and agglomeration VF, the reconstruction process starts by randomly picking a location within the image as the center of agglomeration. Next, particles, sampled from a $N(8,2)$ pixel distribution, are added sequentially around the center location within a pre-specified distance to form the agglomerations. An evolutionary algorithm is implemented to optimize the agglomeration sizes for the desired volume fractions. To obtain realistic agglomerations the center of the agglomeration is tweaked occasionally to reconstruct non-circular shapes. Finally, for the remaining VF, difference between total VF and agglomeration VF, isolated particles are added randomly into the image. Example of reconstructions with specified characteristics are given in Fig.2.

2.3. Interphase Percolation and Design of Experiments

2.3.1. Microstructure Space

In this study, we created a design of experiment (DOE) space of varying microstructure characteristics. Specifically, we considered three total volume fraction (TVF) cases of 2%, 5%, and 8%. For each TVF, we incrementally varied the dispersed volume fraction (DVF) and adjusted number of agglomerations (#agg) from 1 to 6. An example of reconstructed cases for the 2% TVF are presented in Table 1. A similar approach was implemented for 5% (31 characteristics) and 8% (49 characteristics) TVF, with 4-5 replicate images for each configuration, leading to a total of 461 reconstructed images. The binary microstructure property setup remained consistent across cases: the Young's modulus (E) of the matrix and filler are 3.5 GPa and 70 GPa, respectively, while the yield stress for the filler is 132.9 MPa, and the filler is presumed to behave linearly in the small-strain region.

2.3.2. coupled gradient interphase

In coupled gradient interphase scenario, the normalized Young's modulus relative to the matrix value (NormE) and delta Tg were associated, following the same interphatial gradient equation. Slow decay (beta=0.03) and fast decay (beta=0.075) coupled gradient interphase were modeled. *The two beta value were selected according to decay rate of NormE found in the sandwich model and the local delta Tg enhancement range revealed by AFM.* Coupling the two variables together through on of their decay rate aiming at forming a simplified representation for FEA input. Continuous property values were then digitized into 10 bins. Fig.2(a) and Fig.2(b) display examples of NormE and delta Tg values in the slow and fast decay interphase schemes, based on the same microstructure. Coupled gradient interphase have the advantage of shared bins for delta Tg and E, which reduces the number of input layers required for FEA.

2.3.3. decoupled gradient interphase

To achieve more precise modeling, we developed a decoupled gradient interphase scheme, allowing NormE and delta Tg to have different decay rates based on experimental observations. Specifically, NormE follows a faster decay rate, same as the value in the fast coupled

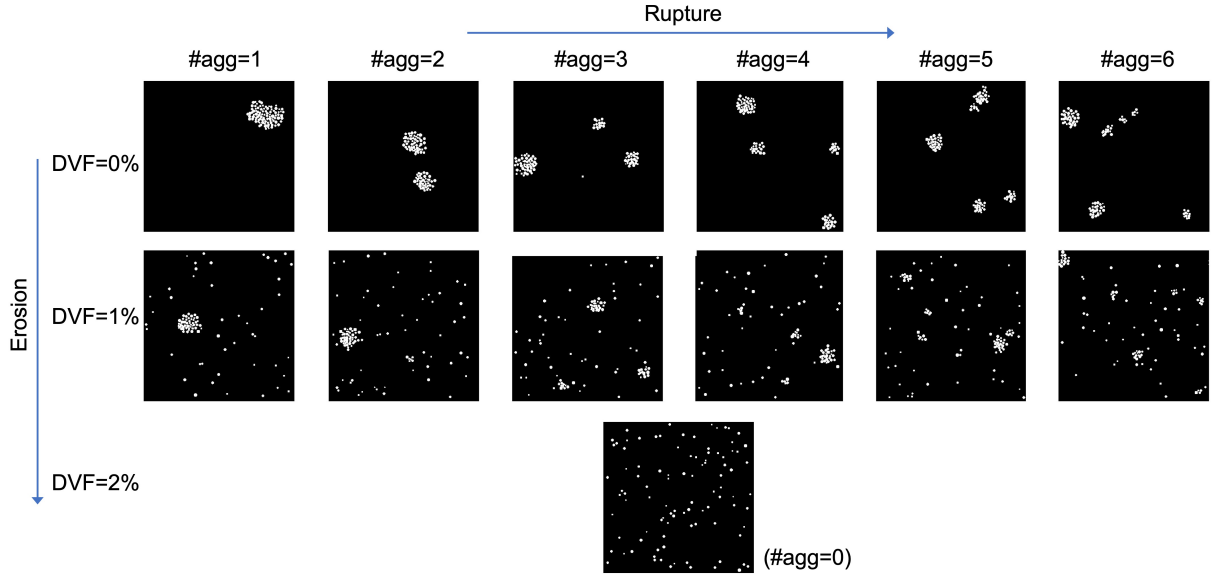


Figure 3: reconstructed microstructures for total volume fraction 2% demonstrating the concepts of erosion of agglomerates into individual isolated particles and rupture of large agglomerates into smaller, distributed ones, forming two axes of our microstructural variability. DVF refers to dispersed volume fraction and #agg refers to the number of agglomerates in each image.

gradient, while ΔT_g adheres to a slower decay rate seen in the slow coupled gradient. As a result, NormE and yield stress are independent and forming distinct bins, as Fig.1(d) shows. In this configuration, more than 50 combination of digitized stiffness and T_g are formed, increasing the complexity of the model. A detailed list of NormE and ΔT_g value in each bins for this example can be find in supplementary material.

2.3.4. uniform interphase

While gradient interphases offer a more granular explanation of local properties compared to uniform interphases, conducting FEA simulations with gradient interphases is computationally intensive and resource-demanding due to the higher level of structural detail. Therefore, we applied the concept of gradient interphase to propose a simplified uniform interphase representation. This model assumes that the uniform interphase contains equal weighted amount of interphase as the gradient model. This framework inherits a portion of information from gradient interphase model, facilitating more efficient simulations while retaining computational cost-effectiveness.

The width of uniform interphase is fixed at 20 pixels (50 nm), whereas NormE and ΔT_g values of the interphase were determined based on weighted amount of interphase of corresponding gradient interphase scheme. Weighted amount of gradient interphase for E was calculated by summing the digitized NormE-1 values across each pixel. The equivalent NormE for the uniform interphase was then computed by dividing the sum by the uniform interphase area. The same process was followed to determine the equivalent ΔT_g . Fig.2(a) and Fig.2(c) illustrate an example of the NormE and yield stress distribution for a

system with slow decay gradient interphase, along with the structure and property values assigned for the microstructure with corresponding equivalent uniform interphase.

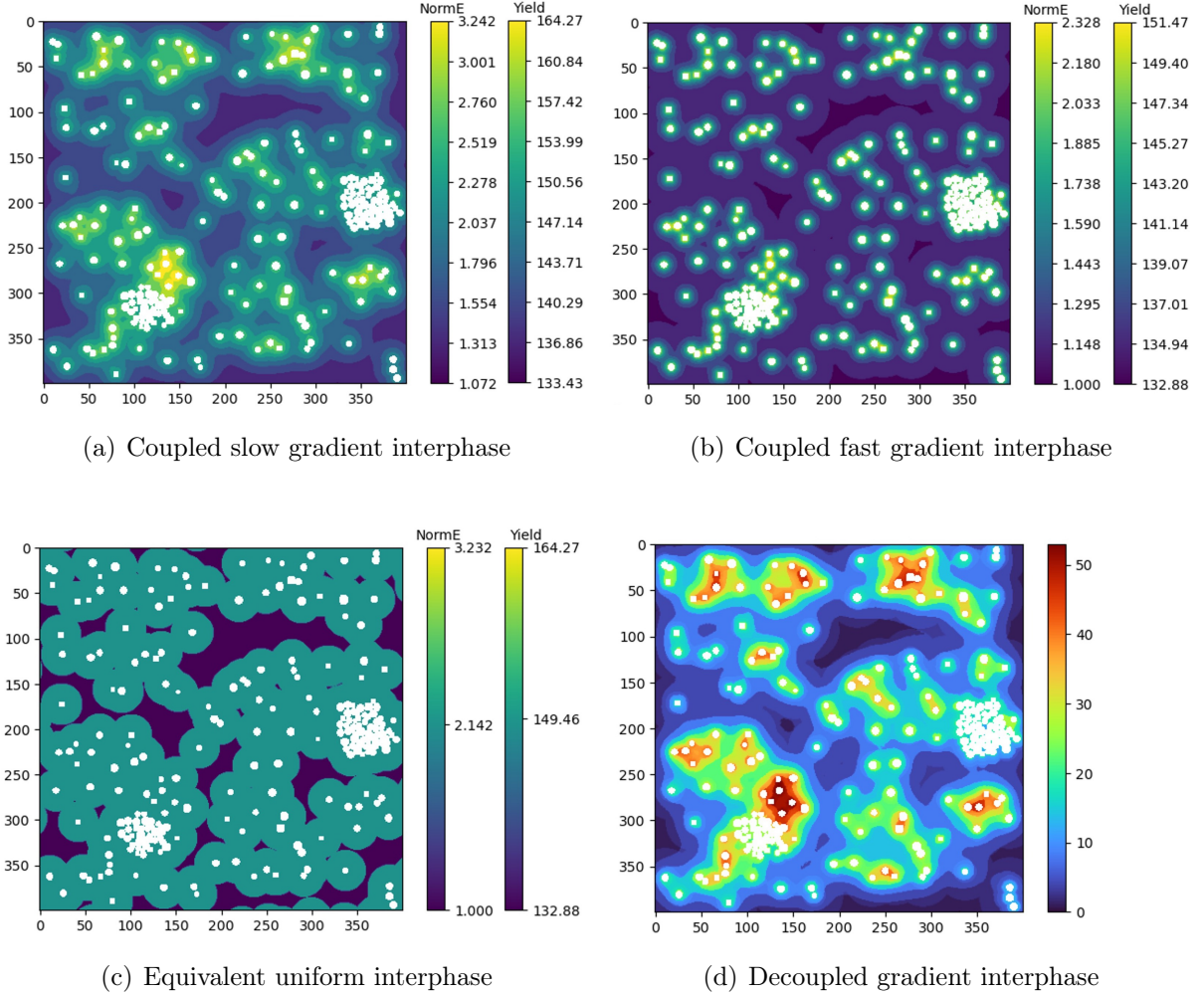


Figure 4: Illustration of a 5% vol fraction (3% DVF) sample with (a)-(c) showing slow and fast decay coupled gradient interphase as well as equivalent uniform interphase with property values and (d) decoupled gradient interphase with distribution of bins only. Color bars in (a),(b) list normalized modulus (NormE) and yield stress value in their 10 bins; colorbar in (c) shows value in matrix(bottom), uniform layer(middle), and maximum value in the corresponding slow gradient case(top) as a reference; Value in color bar of (d) is the layer index (see text for description)

3. Results and Discussion

Stiffness(E) of the system and yield strength are extracted from raw stress-strain data to characterize the system. We developed an algorithm to distinguish between the linear and turning regions, where the discrete data points are fitted using linear regression and a third-order least squares polynomial fit. The slope of the linear region is computed as E ,

while the 0.2% offset method is used to identify the yield point. Graphical illustration and details about E and yield calculations are included in supplementary materials.

3.1. Effect of rupture process

To understand the role of rupture on elasto-plastic properties, Young's modulus and Yield strength obtained from replicates is averaged across dispersed volume fraction(DVF) and plotted against number of agglomerations individually for TVF values of 2%, 5%, and 8%. Figures 5 and 6 compare the E and σ_y performance of fast, slow decay coupled and decoupled gradient interphase within each TVF subgroup, with no-interphase cases serving as a benchmark. In each plot, advancing along the x-axis indicates more rupture, while error bars represent the impact of erosion.

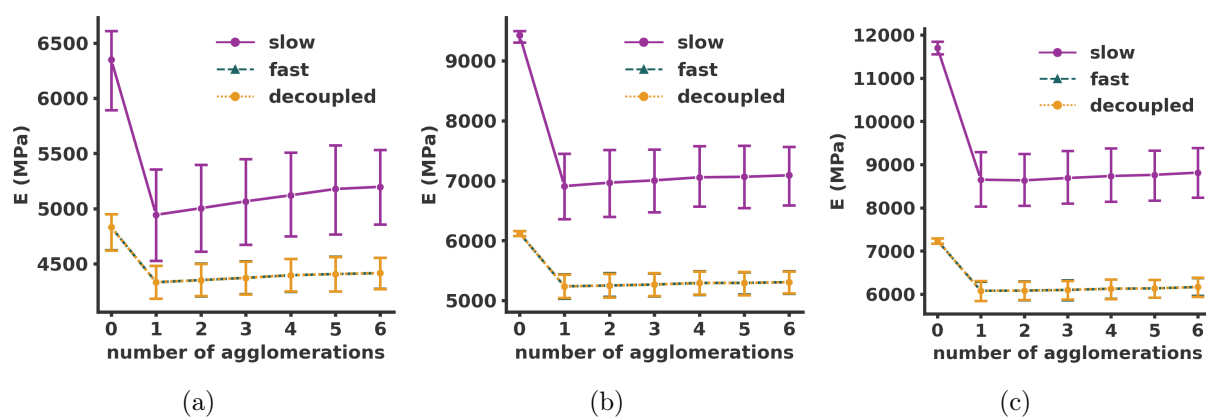


Figure 5: (a) Young's modulus-Dispersed VF relation of total VF 8% cases. (b) Comparing slow gradient and its equivalent uniform interphase behavior. The solid and dashed lines approach each other as the dispersed VF increases, indicating that the uniform interphase approximation is better with more dispersed particles and otherwise underestimates the response. In both plots, the error bar represents the property variability for agglomeration values ranging from 1 to 6, thus the impact of the concept of rupture. The horizontal axis of dispersed volume fraction represents erosion.

In the decoupled gradient interphase scheme, although local yield strength have slower decay rate than coupled fast decay interphase scheme, the bulk stiffness data points between the two schemes highly overlap, suggesting that the elastic property are not affected by the local yield remarkably. The highly comparable behavior of the two schemes implies that the elastic response of real-life PNCs system, which are likely to be decoupled, can be simplified to a corresponding coupled strategy to perform time- and cost-effective simulations. Furthermore, as we aim to simplify the model while retaining accuracy, we also validate the performance of our equivalent uniform interphase scheme. As shown in Fig.4(b), the estimates from equivalent uniform interphase scheme are comparable to those of the corresponding gradient interphase schemes. For material systems with high particle loading and dispersion, the approximations closely imitate gradient interphase behavior. However, in agglomerated and poorly dispersed systems, it tends to underestimate stiffness, with the worse predicted case having an error of of 6.2 %.

To summarize, the DVF is the determining factor for PNCs' stiffness, while agglomerated VF has a minor impact. The erosion of particles from agglomerates significantly promotes property improvement. Efforts to break agglomeration to smaller pieces are not particularly effective unless most of the particles are already clumped. The coupled gradient interphase with desired elastic property serves as a valid substitute for the decoupled gradient interphase when studying stiffness. The equivalent uniform interphase model further provides a reasonable estimation of the gradient interphase in heavily loaded dispersed system.

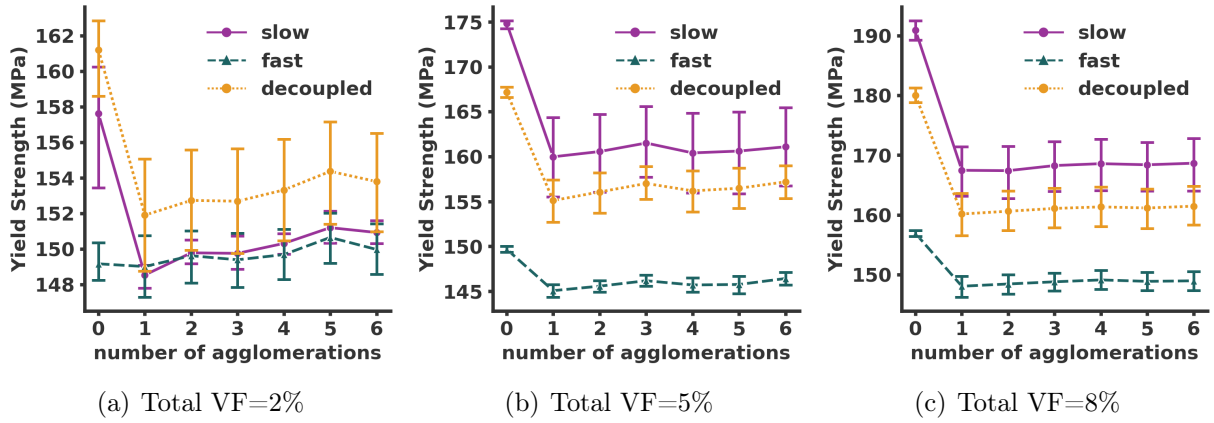


Figure 6: Visualization of Yield strength-dispersed VF relation of (a) 2% total VF, (b) 5% total VF and (c) 8% total VF, respectively. Entanglement between the curves and the consistently changing slope is attributed to the competition between interphase percolation and the surface concentration zone induced by the existence of particles and interphase. Shaded region in c is the threshold of this competition and stress localization are shown on microstructures in Fig.6.

For no-interphase systems, Young's modulus remain practically unchanged with respect to both erosion and rupture. The slight downward trend in the "no-interphase" scenario suggests that agglomerates contribution more to E than isolated particles in the absence of an interphase. However, with an interphase present, increasing erosion becomes the primary factor in promoting stiffness for both fast and slow decay gradient interphase schemes. Increasing the DVF through erosion leads to stable and significant stiffness enhancement. Erosion benefits the slow decay more than fast decay due to its broader interphase range. The interphase area of eroding particles and clusters can sufficiently interact with each other, forming a high-level compound effect that increases local stiffness. Meanwhile, rupture serves as a secondary factor, mainly influencing systems with few or no isolated particles. In such cases, highly ruptured systems exhibit slightly higher Young's modulus, while systems with fewer and larger clusters display relatively lower modulus. In fast decay and systems with lower VF, the role of the number of agglomerations is less noticeable. For the 2% and 5% VF subgroups, similar patterns are observed, with overall lower stiffness for lower VF values (supplementary figure S5).

3.2. Effect of erosion process

To understand the role of erosion process on elasto-plastic properties, Young's modulus and Yield strength obtained from replicates is averaged across number of agglomerations and plotted against dispersed volume fraction, individually for TVF values of 2%, 5%, and 8%. Figures 7 and 8 compare the E and σ_y performance of fast, slow decay coupled and decoupled gradient interphase within each TVF subgroup, with no-interphase cases serving as a benchmark. In each plot, advancing along the x-axis indicates more erosion, while error bars represent the impact of rupture.

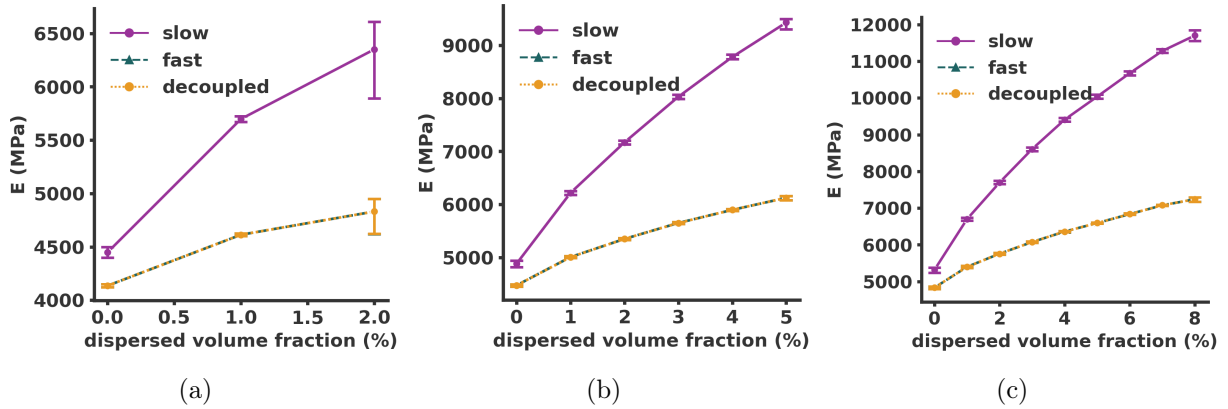


Figure 7: (a) Young's modulus-Dispersed VF relation of total VF 8% cases. (b) Comparing slow gradient and its equivalent uniform interphase behavior. The solid and dashed lines approach each other as the dispersed VF increases, indicating that the uniform interphase approximation is better with more dispersed particles and otherwise underestimates the response. In both plots, the error bar represents the property variability for agglomeration values ranging from 1 to 6, thus the impact of the concept of rupture. The horizontal axis of dispersed volume fraction represents erosion.

4. Discussion

While local properties are the exclusive determining factor for stiffness, the yield response of PNCs is more complex. This complexity can be interpreted as a competition between local fortification due to interphase percolation and the distribution of stress concentration zones. Fig.5 shows the yield response of five interphase schemes at 2%, 5%, and 8% total volume fraction, with error bars representing the range of different numbers of agglomeration (rupture). Observations including importance of erosion, effect of rupture in low dispersion, and difference between fast and slow decay gradient interphase remain visible, as demonstrated in the previous section. However, several notable observation emerge due to fluctuations in stress concentration. We identify two competing processes that take part in the yielding mechanism of material system of PNCs under consideration. The first one is local stress stress distribution in linear regime which can be quantified by full field stress concentration distribution up to limit of proportionality. Zones with higher stress concentration values are prone to undergo local yielding at macro-stress values below macro yield strength point of

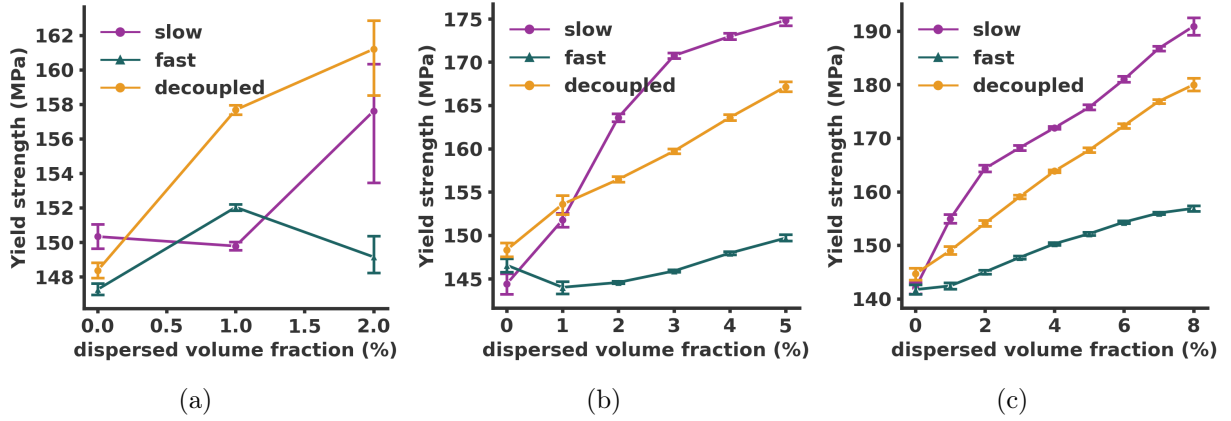


Figure 8: (a) Young’s modulus-Dispersed VF relation of total VF 8% cases. (b) Comparing slow gradient and its equivalent uniform interphase behavior. The solid and dashed lines approach each other as the dispersed VF increases, indicating that the uniform interphase approximation is better with more dispersed particles and otherwise underestimates the response. In both plots, the error bar represents the property variability for agglomeration values ranging from 1 to 6, thus the impact of the concept of rupture. The horizontal axis of dispersed volume fraction represents erosion.

the given microstructure. More precisely, when local stress value reaches local yield limit we will see local yielded regions. However, the local yield limits are determined by the graded yield interphase. Yield interphase percolation is the process that acts to resist local yielding. To explain the trends we see for incremental changes in macro yield strength values with increase in dispersion with erosion and rupture process, we need to understand how these two phenomena, namely linear local stress concentration zones (LLSCZ) and yield interphase percolation, evolve with dispersion.

4.1. Mechanistic insight

Generally, higher stress concentration factors and larger stress concentration zones induce the material to yield. Although this is countered by local yield gradients that provide higher local yield threshold. When the DVF is low, the mean nearest neighbor distance is too large to form sufficient compound effect, so local stress concentration dominates over interphase percolation. This leads to a counteractive bulk yield stress, which can fall below the corresponding no-interphase scheme. Fig. 6(b)(d), and fig.(f),(h) show Mises stress of two examples that have lower macroscale yield in fast decay scheme (Fig6(b) and (f)) than no-interphase scheme (Fig6(d) and (h)). In the no-interphase scheme, both cases have very low local stress concentrations, which are insufficient to affect bulk yield strength notably. In contrast, examples of the fast gradient scheme exhibit higher value locally in both two microstructures, resulting the material yield easier. As the erosion continues, all four series of different interphase schemes show ascending yield stress, exceeding the no-interphase benchmark after reaching 1% DFV for uniform interphase, decoupled, and slow gradient schemes, and about 3% for the fast gradient scheme. During this process, the slow gradient scheme shows a Characteristic plateau, as filled in green in Fig.5. Fig6(a) and (e) show

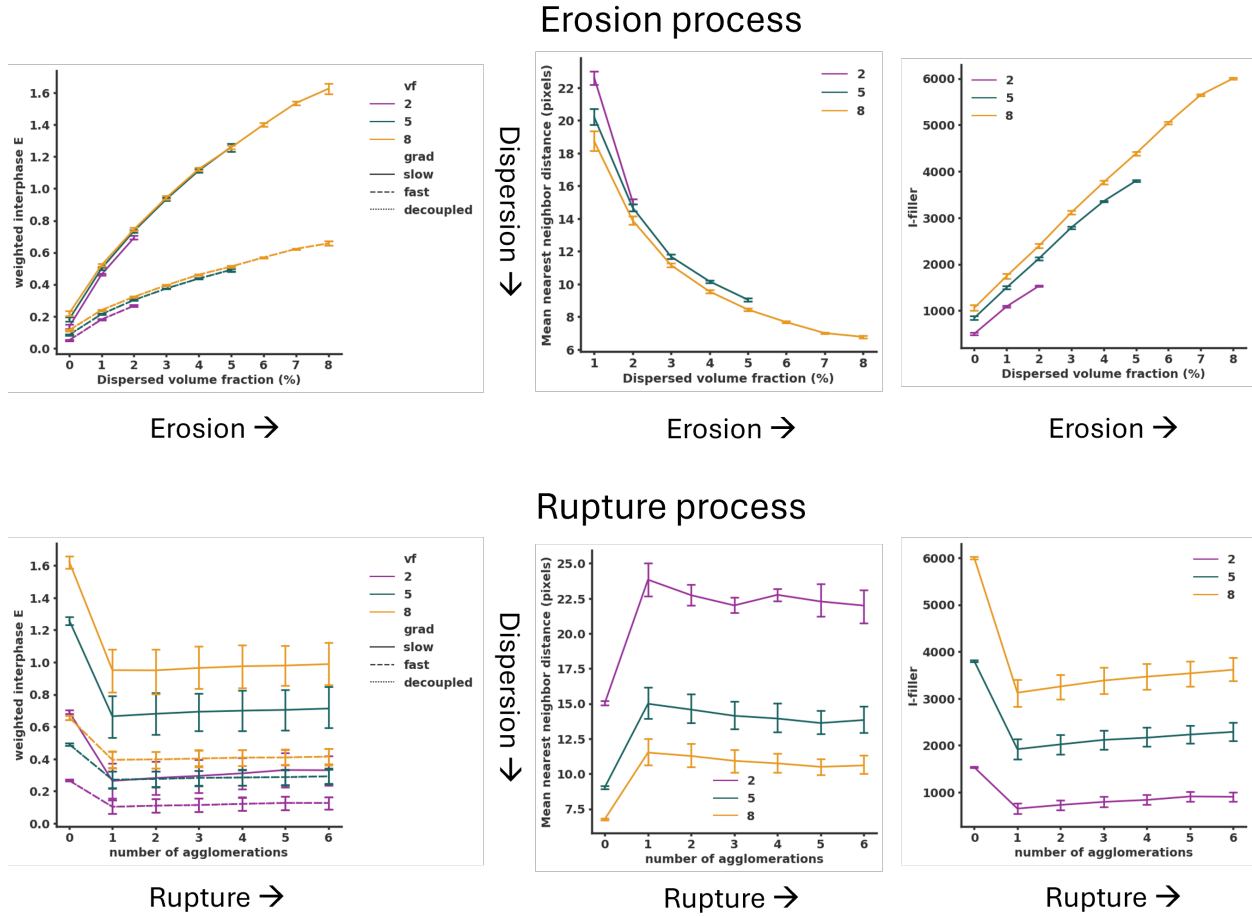


Figure 9: intermediate microstructure descriptors to explain mechanistic behaviour

Mises stress for two data points before (a) and after (e) the plateau in 8% VF. Clearly, both the area and value of local stress have greatly increased, canceling out the compound effect brought by erosion. In other words, as local stress concentration/zone grow catches up with local yielding threshold, the promoting of bulk yield stress pulses and form the plateau. Comparatively, the decoupled gradient interphase curve in fig.5 doesn't show signs for any plateau. Fig.6(c) and (g), which display same microstructures as Fig(a) and (e) but with a decoupled scheme, further explain the mechanism. In these two plots, the stress concentration zones are much narrower than those in slow gradient schemes shown in (a) and (e) because the decoupled scheme has faster decay E . Such small stress concentration zones fail to catch up with the threshold given by the compound effect, resulting the consistent dominant of compound effect and forming a linear behavior throughout the erosion process. A similar linear trend is also observed inspecting the equivalent uniform interphase behavior. Despite having the same amount of interphase as the slow gradient scheme, it shows a flatter plateau since the width of the uniform interphase is controlled to be 50nm.

Due to the obstruction of local stress concentration, using a uniform or a coupled gradi-

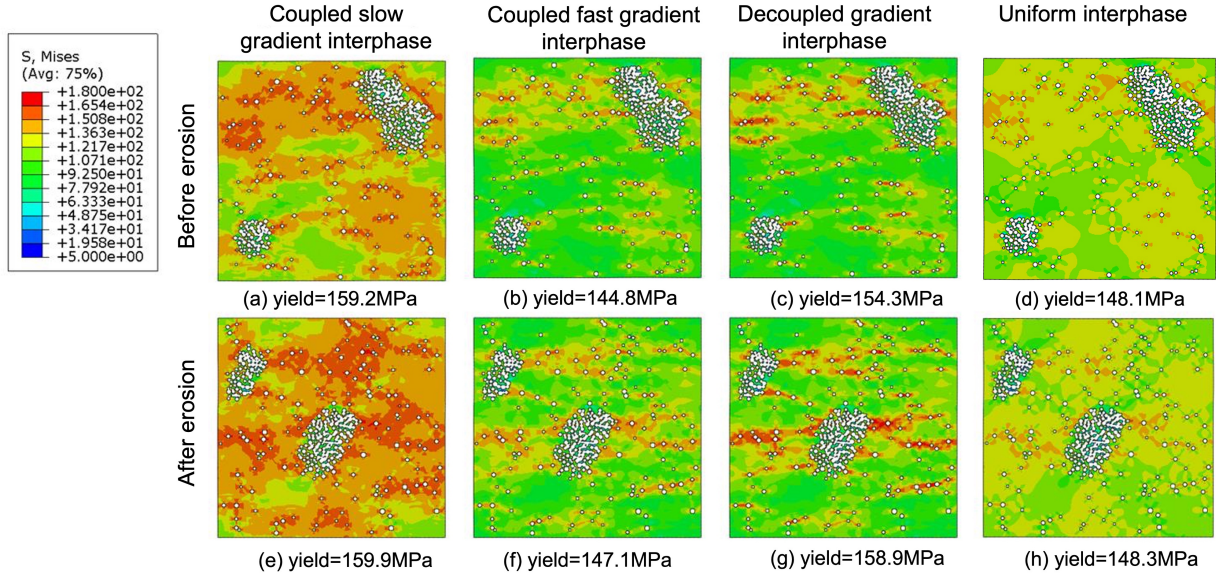


Figure 10: Mises stress of total VF=8%, dispersed VF=2%, number of agglomeration=2% (first row) and total VF=8%, dispersed VF=3%, number of agglomeration=2% (second row). Column 1-4 are slow gradient, fast gradient, decoupled gradient and no interphase schemes, respectively.

ent interphase to simplify decoupled gradient in modeling is case-sensitive and not always promising. However, the linear trend observed at 8% VF in decoupled series suggests the potential of adapting a simple fitting method to predict material yield stress based on scarce stress-strain datapoints.

Overall, the intricate behavior of yield stress discloses a competition between local yielding threshold promoted by interphase and the stress concentration caused by stiffness changes. Plateaus and intersections may occur as erosion progresses, which requires attention when designing PNCs. The performance of different interphase schemes can serve as a reference for wet lab experiments when designing PNCs. It may also provides evidence to the existence of gradient interphases and their patterns when compared to experimental outcomes.

To gain deeper insight into the underlying relationship between the microstructure, interphase schemes of PNCs, and their elastoplastic response, we define and calculate three descriptors to describe a PNC system: I-filler, weighted amount of interphase, and mean nearest neighbor distance (MNND). A brief explanation of these descriptors are provided in Table.1. More detailed definitions and calculation methods are included in supplementary material.

Fig.7 shows the relationship between the three descriptors and two properties. Fig.7(a) reveals that the E of the PNCs exponentially decay with the MNND; however, different interphase schemes can possess different decaying parameters. As particles or agglomerates become less crowded, MNND increases, eliminating the chance of having compounding effect, which leads to a reduction in property. The exponential shape of the curve is formed since

Table 1: Definition and description of descriptor studied

| Descriptor | Definition | Implication |
|--------------------------------|---|---|
| I-filler | Total perimeter of filler phase | Amount of particle surface that is exposed to matrix phase and leading to the formation of interphase. |
| Weighted amount of interphase | Summation of E in a microstructure with interphase for each pixel subtracted by summation of E in no interphase scheme for each pixel for the same microstructure | Relevant extent of property increased in the whole system due to single body effect and compound effect |
| Mean nearest neighbor distance | The mean of all particles/agglomerates' nearest neighbor distance base on edge-to-edge distance | Crowding level of the system. |

the slop of property decaying with MNND is smaller in sparser systems since there are fewer compound effect to begin with.

It can be observed that although I-filler and weighted amount of interphase are both positively related to stiffness, the mechanisms behind differ: I-filler measures the amount of particle/aggregate edges exploded outside, containing information about amount of particle and the potential to promote matrix's property. Therefore, for different interphase settings, the I-filler-E relationship may follow different quadratic curves depending on the power of interphase acting on a given I-filler. However, all data points can be fitted in one single curve for the same interphase scheme, regardless of VF, as I-filler already carries that information. One example is in Fig.7(b), where the slow decay gradient interphase form a more rapidly increasing quadratic curve than fast decay gradient interphase. Yet, the weighted amount of interphase precisely records the degree to which the matrix's property are enhanced, but it does not contain any information about the particles themselves. In Fig.7(c), when examining different interphase settings and filler VF together, three linear groups are identified, each corresponding to one filler volume fraction. The small separation between the three groups shows the effect of particles. Since we observe a complete overlap between the two interphase schemes and that they form a same linear trend for each VF, it is safe to conclude that the amount of interphase has a linear correlation with material stiffness, with only a limited additive effect brought by the particles. The stiffness of a PNC system could be directly predicted without running a full simulation, given the particle fraction and weighted amount of interphase.

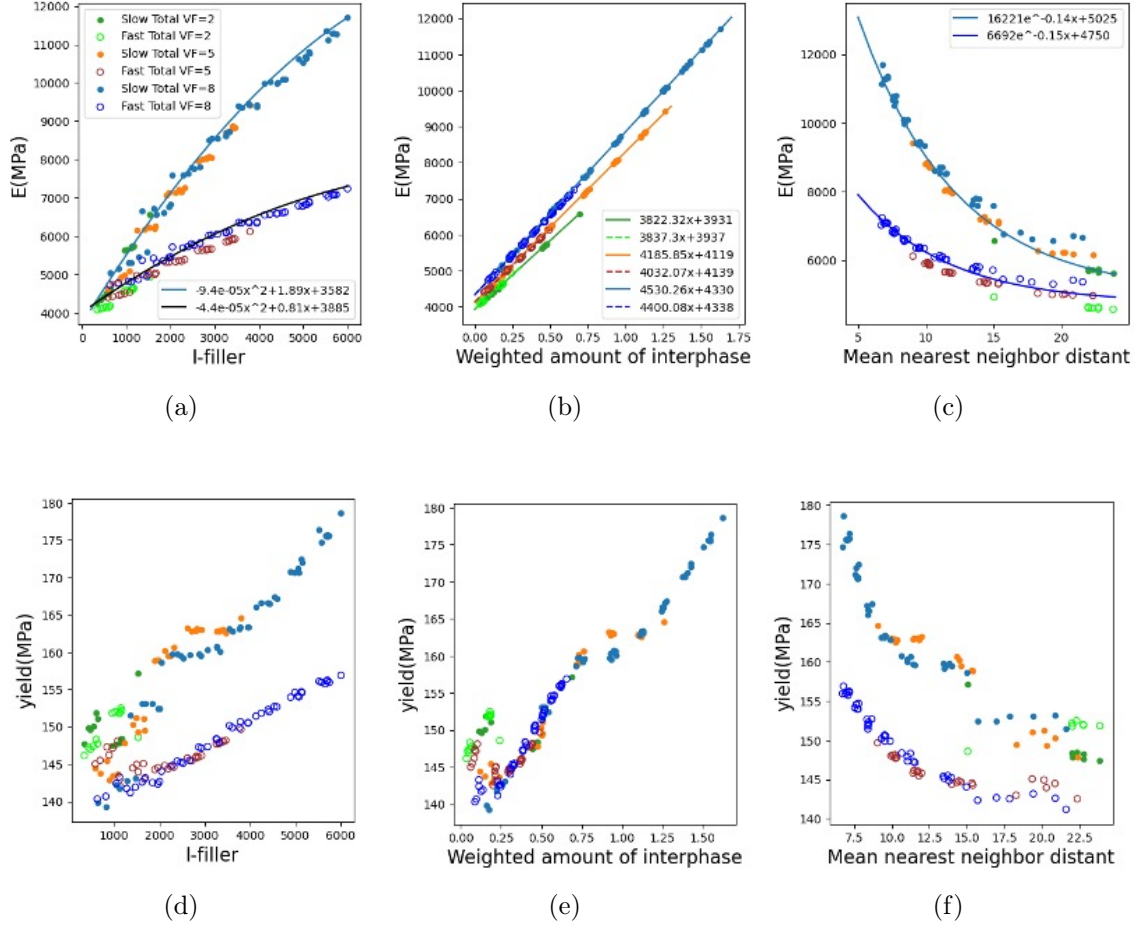


Figure 11: Relation of I-filler(first column), weighted amount of interphase(second column), and mean nearest neighbor distance(Third column) with E(first row) and Yield stress(second row)

5. Conclusion

This study examines elastoplastic behavior of PNCs across various interphase schemes and dispersion levels, further verifying the critical role of the interphase in reinforcing the mechanical properties of PNCs. The erosion of agglomerated particle facilitates the exposure of interphase, thereby augmenting both stiffness and yield more effectively rupture. Rupture exerts a minor effect, impacting the system primarily when most fillers are in an agglomerated state. For stiffness, the compound effect induced by the interaction of gradient interphase enhances local properties and directly contributes to macro-scale stiffness. Notably, stiffness is found to have a linear correlation with the weighted amount of interphase, suggesting a novel predictive approach for bulk stiffness by simply calculating the weighted amount of interphase, rather than running repetitive simulations. Regarding yield stress, the interphase engages in a dynamic competition with local stress zones/concentrations, resulting in intricate bulk yield strength behavior. The results indicate that plateaus can form when attempting to erode any cluster, and, under certain structural conditions, the

interphase contribution can be counterproductive, giving values that are lower than those of systems without an interphase. From a model design perspective, a coupled gradient interphase, which is simpler and faster for computation, can replace a decoupled gradient interphase for stiffness measurement, but not for nonlinear properties due to its complexity. The proposed equivalent uniform interphase provides a reasonable estimation of its corresponding gradient interphase, especially for systems with higher total and dispersed volume fractions, making it a viable alternative for the rapid calculations. Overall, this work provides computational evidence that can inform the design of polymer nanocomposites and deepen the understanding of the role and configuration of interfacial gradients.

Acknowledgements

The authors would like to gratefully acknowledge the support of AFOSR (Grant No: FA9550-18-1-0381) for this work. The authors also thank Prof. Linda Schadler from the University of Vermont for providing the experimental images of PMMA-SiO₂ nanocomposites. We also thank many insightful discussions with Dr. Richard Sheridan and Dr. Marc Palmeri from Duke University, and Gourav Pravin Kumbhojkar from Northwestern University for helping with the simulations.

References

- [1] A. Dorigato, A. Pegoretti, A. Penati, et al., Linear low-density polyethylene/silica micro-and nanocomposites: dynamic rheological measurements and modelling, *Express Polymer Letters* 4 (2) (2010) 115–129.
- [2] J. Oberdisse, Aggregation of colloidal nanoparticles in polymer matrices, *Soft matter* 2 (1) (2006) 29–36.
- [3] D. Li, R. B. Kaner, How nucleation affects the aggregation of nanoparticles, *Journal of Materials Chemistry* 17 (22) (2007) 2279–2282.
- [4] P. Cassagnau, Melt rheology of organoclay and fumed silica nanocomposites, *Polymer* 49 (9) (2008) 2183–2196.
- [5] K. Matsushige, S. Radcliffe, E. Baer, The pressure and temperature effects on brittle-to-ductile transition in ps and pmma, *Journal of Applied Polymer Science* 20 (7) (1976) 1853–1866.
- [6] J.-W. Wee, A. Chudnovsky, B.-H. Choi, Brittle–ductile transitions of rubber toughened polypropylene blends: a review, *International Journal of Precision Engineering and Manufacturing-Green Technology* 11 (4) (2024) 1361–1402.
- [7] B. J. Ash, R. W. Siegel, L. S. Schadler, Mechanical behavior of alumina/poly (methyl methacrylate) nanocomposites, *Macromolecules* 37 (4) (2004) 1358–1369.
- [8] R. Peng, H. Zhou, H. Wang, L. Mishnaevsky Jr, Modeling of nano-reinforced polymer composites: Microstructure effect on young’s modulus, *Computational Materials Science* 60 (2012) 19–31.
- [9] G. Odegard, T. Clancy, T. Gates, Modeling of the mechanical properties of nanoparticle/polymer composites, in: *Characterization of Nanocomposites*, Jenny Stanford Publishing, 2017, pp. 319–342.
- [10] X. Li, M. Zhang, Y. Wang, M. Zhang, A. Prasad, W. Chen, L. Schadler, L. C. Brinson, Rethinking interphase representations for modeling viscoelastic properties for polymer nanocomposites, *Materialia* 6 (2019) 100277. doi:<https://doi.org/10.1016/j.mtla.2019.100277>. URL <https://www.sciencedirect.com/science/article/pii/S2589152919300730>
- [11] P. Rittigstein, R. D. Priestley, L. J. Broadbelt, J. M. Torkelson, Model polymer nanocomposites provide an understanding of confinement effects in real nanocomposites, *Nature materials* 6 (4) (2007) 278–282.
- [12] C. J. Ellison, J. M. Torkelson, The distribution of glass-transition temperatures in nanoscopically confined glass formers, *Nature materials* 2 (10) (2003) 695–700.
- [13] M. Zhang, S. Askar, J. M. Torkelson, L. C. Brinson, Stiffness Gradients in Glassy Polymer Model Nanocomposites: Comparisons of Quantitative Characterization by Fluorescence Spectroscopy and Atomic Force Microscopy, *Macromolecules* 50 (14) (2017) 5447–5458, publisher: American Chemical Society. doi:10.1021/acs.macromol.7b00917. URL <https://doi.org/10.1021/acs.macromol.7b00917>
- [14] E. U. Mapesa, D. P. Street, M. F. Heres, S. M. Kilbey, J. Sangoro, Wetting and chain packing across interfacial zones affect distribution of relaxations in polymer and polymer-grafted nanocomposites, *Macromolecules* 53 (13) (2020) 5315–5325.
- [15] M. Zhang, Y. Li, P. V. Kolluru, L. C. Brinson, Determination of Mechanical Properties of Polymer Interphase Using Combined Atomic Force Microscope (AFM) Experiments and Finite Element Simulations, *Macromolecules* 51 (20) (2018) 8229–8240, publisher: American Chemical Society. doi:10.1021/acs.macromol.8b01427. URL <https://doi.org/10.1021/acs.macromol.8b01427>
- [16] M. Zhang, Local mechanical properties characterization of soft polymeric material via atomic force microscopy nanoindentation and finite element simulations, Ph.D. thesis (2018).
- [17] B. Du, O. K. Tsui, Q. Zhang, T. He, Study of elastic modulus and yield strength of polymer thin films using atomic force microscopy, *Langmuir* 17 (11) (2001) 3286–3291.
- [18] P. V. Kolluru, M. D. Eaton, D. W. Collinson, X. Cheng, D. E. Delgado, K. R. Shull, L. C. Brinson, Afm-based dynamic scanning indentation (dsi) method for fast, high-resolution spatial mapping of local viscoelastic properties in soft materials, *Macromolecules* 51 (21) (2018) 8964–8978.
- [19] R. Bostanabad, Y. Zhang, X. Li, T. Kearney, L. C. Brinson, D. W. Apley, W. K. Liu, W. Chen, Computational microstructure characterization and reconstruction: Review of the state-of-the-art techniques, *Progress in Materials Science* 95 (2018) 1–41.

Supplementary Figures

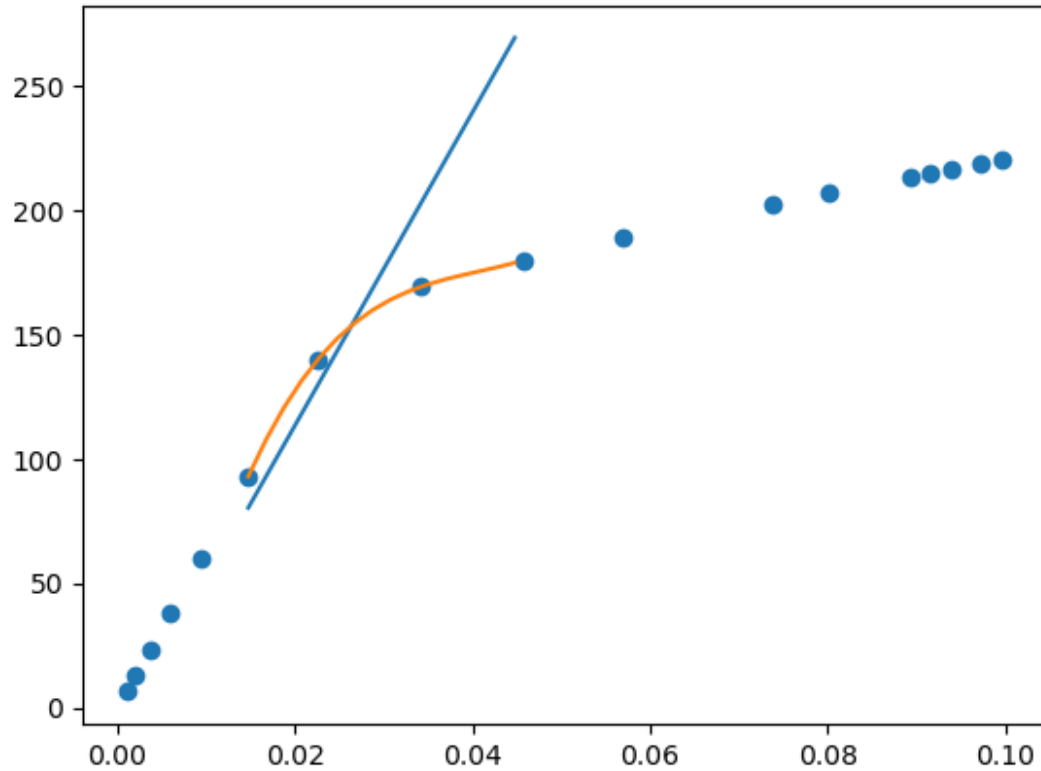


Figure S1: Illustration of stress-strain data points, yielding region fitting and 0.2% offset method

Steps of E and yield calculation:

1. Find the linear region. Start from the first point, when $(\text{gradient of point } n+1 / \text{gradient of point } n) > 1.03$, break, linear region ends.
2. Calculate E by take average of the gradients of the points in linear region found in step 1.
3. Find the yielding region: Start from the first point outside linear region, when $(\text{gradient of point } n+1 / \text{gradient of point } n) < 1.03$, break, fitting region ends.
4. Fit the yielding region using 3rd order polynomial.
5. Perform a 0.2% strain offset of the linear region line.
6. Find the intersection of the fitted curve in step 4 and offset line in step 5. Yield stress is recorded as the stress value of the intersection.